Fowler, E., Kong, C., Hancox, J., & Cannell, M. (2018). Late Ca2+ Sparks and Ripples During the Systolic Ca2+ Transient in Heart Muscle Cells. *Circulation Research*, *122*, 473-478. https://doi.org/10.1161/CIRCRESAHA.117.312257

**SHORT COMMUNICATION**

# Late $Ca^{2+}$ Sparks and Ripples During the Systolic $Ca^{2+}$ Transient in Heart Muscle Cells

Ewan D. Fowler, Cherrie H.T. Kong, Jules C. Hancox & Mark B. Cannell

School of Physiology, Pharmacology & Neuroscience, Faculty of Biomedical Sciences, University of Bristol, University Walk, Bristol BS8 1TD, United Kingdom.

***Running title:*** Late $Ca^{2+}$ Sparks and Ripples in Heart





**Subject Terms**:
Basic Science Research
Calcium Cycling/Excitation-Contraction Coupling
Myocardial Biology
Physiology

**Address correspondence to**:
Dr. Mark B Cannell
School of Physiology, Pharmacology & Neuroscience
Faculty of Biomedical Sciences
University of Bristol
University Walk
Bristol BS8 1TD
+44 (0) 117 331 1894
United Kingdom
mark.cannell@bristol.ac.uk

**In November 2017, the average time from submission to first decision for all original research papers submitted to *Circulation Research* was 11.99 days.**

## ABSTRACT

***Rationale:*** The development of a refractory period for $Ca^{2+}$ spark initiation after $Ca^{2+}$ release in cardiac myocytes, should inhibit further $Ca^{2+}$ release during the action potential (AP) plateau. However, $Ca^{2+}$ release sites that did not initially activate, or which have prematurely recovered from refractoriness might release $Ca^{2+}$ later during the AP and alter the cell-wide $Ca^{2+}$ transient.

***Objective:*** To investigate the possibility of late $Ca^{2+}$ spark (LCS) activity in intact isolated cardiac myocytes using fast confocal line scanning with improved confocality and signal to noise.

***Methods and Results:*** We recorded $Ca^{2+}$ transients from cardiac ventricular myocytes isolated from rabbit hearts. APs were produced by electrical stimulation and rapid solution changes were used to modify the L-type $Ca^{2+}$ current. After the upstroke of the $Ca^{2+}$ transient, late $Ca^{2+}$ sparks (LCS) were detected which had increased amplitude compared to diastolic $Ca^{2+}$ sparks. LCS are triggered by both L-type $Ca^{2+}$ channel activity during the action potential plateau, as well as by the increase of cytosolic $Ca^{2+}$ associated with the $Ca^{2+}$ transient itself. Importantly, a mismatch between SR load and L-type $Ca^{2+}$ trigger can increase the number of LCS. The likelihood of triggering a LCS also depends on recovery from refractoriness that appears after prior activation. Consequences of LCS include a reduced rate of decline of the $Ca^{2+}$ transient and, if frequent, formation of microscopic propagating $Ca^{2+}$ release events ($Ca^{2+}$ ripples). $Ca^{2+}$ ripples resemble $Ca^{2+}$ waves in terms of local propagation velocity but spread for only a short distance due to limited regeneration.

***Conclusions:*** These new types of $Ca^{2+}$ signalling behaviour extend our understanding of $Ca^{2+}$ mediated signalling. LCS may provide an arrhythmogenic substrate by slowing the $Ca^{2+}$ transient decline as well as by amplifying maintained $Ca^{2+}$ current effects on intracellular $Ca^{2+}$ and consequently $Na^{+}/Ca^{2+}$ exchange current.



**Keywords:**

Heart, $Ca^{2+}$ sparks, excitation-contraction coupling, cytosolic $Ca^{2+}$, calcium signaling, cardiomyocyte, cardiac myocyte


**Nonstandard Abbreviations and Acronyms:**

| | |
|---|---|
| NT | Normal Tyrode superfusion solution |
| LCS | late $Ca^{2+}$ sparks |
| Jsr | junctional sarcoplasmic reticulum |
| AP | Action potential |
| ECC | excitation-contraction coupling |
| LTCC | L-type $Ca^{2+}$ channels |
| ICC | intraclass correlation coefficient |

## INTRODUCTION

Cardiac excitation-contraction coupling (ECC) is mediated at the cellular level by the near-synchronous activation of ~$10^4$ microscopic $Ca^{2+}$ release events called $Ca^{2+}$ sparks (1, 2). This occurs because the cardiac action potential (AP) opens L-type $Ca^{2+}$ channels (LTCC) in the surface membrane to produce a local increase in $Ca^{2+}$ which in turn opens $Ca^{2+}$-sensitive channels (ryanodine receptors, RyR) in the adjacent junctional sarcoplasmic reticulum membrane (jSR) (3). The spatial restrictions associated with this "local control" mechanism provide this signal transduction pathway both high gain and stability (1, 4) and forms the cornerstone of our current understanding of ECC, explaining the time- and voltage-

dependence of the regenerative $Ca^{2+}$ release process (5-7). $Ca^{2+}$ sparks normally occur with very high probability at the start of the $Ca^{2+}$ transient (8, 9) and $Ca^{2+}$ release during the $Ca^{2+}$ spark is terminated in ~10 ms, probably via SR depletion dependent processes (10). The cytoplasmic $Ca^{2+}$ concentration then returns towards resting levels in a few hundred milliseconds as $Ca^{2+}$ is pumped back into the SR (via SERCA2a) and across the surface membrane (mainly via NCX) (4, 11, 12). This currently accepted view of ECC has led to changes in the time course of $Ca^{2+}$ decline being generally attributed to changes in SERCA2a and NCX activities with smaller contributions from a sarcolemmal $Ca^{2+}$-ATPase and mitochondria (13, 14). However, continued SR release (or leak) should oppose SR re-uptake and slow the time course of the $Ca^{2+}$ transient, as seen in a phospholamban knockout mice with CamKIIδc overexpression (15).

## METHODS

The data that support the findings of this study are available from the corresponding author upon reasonable request.

Ventricular cardiomyocytes from New Zealand White rabbits were field stimulated at 0.5 Hz at 1.2x threshold at 22ºC. To avoid possible problems associated with cell dialysis, whole-cell patch camp techniques were not used. Cell movement artefacts were prevented by adding 10 mmol/L 2,3-butanedione monoxime (BDM) to NT. It should be noted that late $Ca^{2+}$ sparks were also seen in the absence of BDM and at 37ºC (see Online Figure I ). BDM may modify the relative importance of triggers for $Ca^{2+}$ sparks in the experiments shown here (see Online Supplement). Fast block of L-type $Ca^{2+}$ channels was achieved by local superfusion with $Cd^{2+}$ (10 or 100 μmol/L) plus 1 μmol/L sulforhodamine-B in NT from a pressurized micropipette, the fluorescence of which allowed determination of the local concentration of $Cd^{2+}$ (and hence degree of LTCC block).

More extensive Methods are given in the Online Supplement

## RESULTS

By using high sensitivity detectors and improved confocality, we have been able to detect additional $Ca^{2+}$ release events ("late $Ca^{2+}$ sparks") during the entire time course of the cellular $Ca^{2+}$ transient. The left panel in Fig. 1A shows a typical $Ca^{2+}$ transient recorded from a ventricular myocyte using confocal line scanning (9), and the right panel shows a high-pass filtered and contrast enhanced version of this image in which these late $Ca^{2+}$ sparks (LCS) can be seen more clearly. Individual LCS (Fig. 1B) had an increased amplitude compared to diastolic $Ca^{2+}$ sparks (Fig. 1C), but did not exhibit any changes in duration (~40 ms) or spatial full width at half maximum (~1.8 μm) (data not shown). The increase in amplitude of the LCS can be explained by a reduction in cytoplasmic $Ca^{2+}$ buffering power due to cytoplasmic $Ca^{2+}$ binding sites (such as troponin) becoming occupied during the $Ca^{2+}$ transient (14). A simple, obvious, explanation for the genesis of the late $Ca^{2+}$ sparks would be that they arise from jSR that was either not activated during the upstroke of the $Ca^{2+}$ transient or was uncoupled or 'orphaned' (17) from t-tubules (which carry the AP to the cell interior). To examine this idea, we labelled t-tubules (Fig. 1D) and measured the Euclidian distance to the LCS centroid (Fig. 1E) and compared the latencies for the upstroke of the $Ca^{2+}$ transient at LCS sites to overall $Ca^{2+}$ transient latency (Fig. 1F). Perhaps unexpectedly, LCS occurred close to t-tubules and at positions where the $Ca^{2+}$ transient developed with a shorter than average latency ($p<0.05$). This suggests that LCS usually arise from sites that are not 'orphaned' but are, in fact, well coupled, a view also

supported by the presence of an extensive t-tubule network (top and middle panels Fig. 1D) that did not show any signs of the disruption associated with orphaning (17).

Following activation, $Ca^{2+}$ spark sites enter a refractory period (18, 19) which should oppose any secondary activation. The spontaneous $Ca^{2+}$ spark refractory period has been estimated by analysing the inter-$Ca^{2+}$ spark interval from ryanodine-modified rat (18) or CamKIIδc overexpressing mouse (15) myocytes. We performed a similar analysis on LCS sites: Fig. 2A shows two LCS sites with different inter-LCS intervals. Initial LCS (red arrows) followed the AP evoked $Ca^{2+}$ transient with a latency distribution shown as in Fig. 2B. Only a few LCS are seen shortly after the onset of the $Ca^{2+}$ transient but this increases and reaches a peak before declining with a half time of ~500 ms which is very similar to the half time of the whole-cell $Ca^{2+}$ transient (also shown in Fig. 2B behind the histogram bars) in this species at room temperature (20). The time between the first and second LCS (blue arrows Fig. 2A) is shown in Fig. 2C and the amplitude of the second event compared to the first is shown in Fig. 2D. Since LCS amplitude restitution matches the reported rabbit jSR refilling time course (19), jSR refilling probably determines LCS amplitude recovery. In this regard, LCS behave similarly to ryanodine-stimulated diastolic $Ca^{2+}$ sparks (18). By dividing $Ca^{2+}$ spark probability by an exponential fit, the first and second LCS activation probability can be derived (18). It is apparent that the LCS activation probability is (essentially) the same for both the first and second LCS (Fig. 2E) suggesting that recovery from refractoriness is a dominant factor in their genesis –but what is their trigger?

During the long plateau phase of the AP, LTCCs continue to open stochastically (21, 22) and might trigger LCS as individual release sites recover from their refractory period. If this is the case, one might predict that LTCC inhibition should reduce the number of LCS. As illustrated in Fig. 3A, blocking ~75% of LTCCs with extracellular $Cd^{2+}$ (a fast LTCC open-state blocker (23)) paradoxically increased the number of LCS (Fig. 3C). However, straight-forward interpretation of this experiment is complicated by the block of LTCCs during the upstroke of the AP reducing jSR site activation (Fig. 3D). This effect would increase release site availability because fewer sites would then be refractory at later times. Importantly, these data also show that the increased number of LCS produced in this condition make a significant contribution to the time course of the $Ca^{2+}$ transient (Fig. 3B,E). To remove the complication arising from changes in the number of jSR release sites activated during the AP, we rapidly applied a higher concentration of $Cd^{2+}$ just after the upstroke of the $Ca^{2+}$ transient to selectively block later LTCC openings. To show the effect of such early LTCC blockade clearly, we show an exemplar (Fig. 3F) that had a higher rate of LCS production shortly after the upstroke of the $Ca^{2+}$ transient which contributed to an extended rising phase which can be seen under condition of lower SR load (e.g. (21)). The time of arrival and local concentration of $Cd^{2+}$ was measured by fluorescently labelling the solution with sulforhodamine-B which, with the $K_d$ for $Ca^{2+}$ block, allowed us to estimate that ~90% LTCCs should be blocked after the upstroke of the $Ca^{2+}$ transient (Fig. 3G). This reduced the number of LCS, but only by 40% (Fig. 3H) supporting the idea that LCS can also be triggered by the rise in cytosolic $Ca^{2+}$ during the $Ca^{2+}$ transient. As expected, the application of $Cd^{2+}$ shortly after the stimulus and upstroke of the AP had no effect on the amplitude of the $Ca^{2+}$ transient (Fig. 3I) but slightly shortened its duration (Fig. 3G, J), which is likely to be due to AP shortening (24) (due to LTCC blockade) and the reduced number of LCS.

LCS production is a part of a continuum of behaviour that spans the low spontaneous $Ca^{2+}$ spark rate during diastole (~1 per 100 μm/s scanned) to very high rates (~$10^4$ per 100 μm/s) during the upstroke of the $Ca^{2+}$ transient (8, 9). Normally, $Ca^{2+}$ sparks interact weakly (25) but when SR and cytoplasmic $Ca^{2+}$ levels increase, $Ca^{2+}$ waves can develop from the sequential recruitment of $Ca^{2+}$ spark sites (26). The spatio/temporal relationship between LCS site activation (Fig. 4A) was analysed by calculating autocorrelograms (Fig. 4B). In most of our experiments, such autocorrelation analysis showed only a time dependent relationship between spark sites, reflecting the refractory period (Fig. 4C) described earlier. However, in a subset of cells that were more highly $Ca^{2+}$ loaded (Fig. 4D), the autocorrelogram showed multiple peaks indicating that some LCS were both spatially and temporally correlated (Fig. 4E). The right panel of Fig. 4D illustrates the chevron patterns in LCS production that can be seen by eye and analysis of

the 2D autocorrelogram showed an apparent propagation velocity between LCS sites ~114 μm/s (Fig. 4F), similar to typical macroscopic $Ca^{2+}$ wave propagation velocities (26, 27). We call these novel propagating LCS events "$Ca^{2+}$ ripples" as (i) they are smaller in amplitude, (ii) do not propagate over the entire cell and (iii) occur during the declining phase of the $Ca^{2+}$ transient, although they are clearly related to the well-known phenomenon of $Ca^{2+}$ waves which can occur during the diastolic period in cardiac myocytes (3, 26, 27).

## DISCUSSION

The presence of LCS during the normal $Ca^{2+}$ transient has important implications for understanding the complex interplay of SR $Ca^{2+}$ release site activation, refractoriness, SR $Ca^{2+}$ reuptake and triggers for CICR (see Online Figure II). Reduced LTCC activation can not only disrupt the initial phase of $Ca^{2+}$ release, leading to dyssynchrony (28, 29), but also increase the number of LCS which can slow the decline of the $Ca^{2+}$ transient. It is notable that reduced LTCC activation can also occur with pathological changes in t-tubules (30), APs (13) or signal transduction cascades (3). Increased SR leak in a CamKIIδc overexpressing mouse model has been shown to slow the decline of the $Ca^{2+}$ transient and some LCS activity during the $Ca^{2+}$ transient can be seen in Fig. 7 of that paper (15). These results are also consistent with the ability of release sites to recover from refractoriness sufficiently quickly for some fraction to become reactivated either by cytosolic $Ca^{2+}$ or LTCCs. While some uncertainty exists in the relative roles of cytoplasmic $Ca^{2+}$, LTCC and NCX in triggering LCS and their effect on the $Ca^{2+}$ transient time course (an uncertainty compounded by BDM used to inhibit movement artefacts –see Online Supplement) it is clear LCS production will be sensitive to all of these triggers. In the case of heart failure, any increase in LCS production could exacerbate the existing problem of slowed $Ca^{2+}$ re-uptake due to decreased SERCA2a activity (31). Further complexity is added by the changes in $Ca^{2+}$ transient time course also affecting LTCC gating via prolongation of the AP due to NCX-generated current during the declining phase of the $Ca^{2+}$ transient (13) as well as the differential responses of coupled and uncoupled release sites (32).

Under normal conditions, LCS production is initially inhibited by the refractory period following $Ca^{2+}$ spark activation (18), but the time course of recovery is shorter than the duration of the plateau of the AP during which a sizeable LTCC current flows. Thus LCS are more likely to occur late in the AP and by slowing the decline of the $Ca^{2+}$ transient may contribute to the antagonism between inward NCX current and repolarization reserve (13). As illustrated in Online Figure II, some pathological changes in the ECC cycle could increase the probability of LCS which, in turn, may prolong the duration of the $Ca^{2+}$ transient (15) and AP duration. This forms a new positive feedback pathway that will promote AP prolongation and further $Ca^{2+}$ influx via LTCC, further destabilizing $Ca^{2+}$ cycling and increasing all forms of $Ca^{2+}$ leak (33).

While more work is needed to fully explore the implications of the novel results presented here, it is now apparent that SR $Ca^{2+}$ release in the form of late $Ca^{2+}$ sparks can continue at lower rates throughout the cardiac $Ca^{2+}$ transient rather than solely during the upstroke of the $Ca^{2+}$ transient as usually modelled.


## ACKNOWLEDGEMENTS

This work was supported by the British Heart Foundation (grant RG/12/10/29802) and Medical Research Council (MR/N002903/1).


## DISCLOSURES

None.

## REFERENCES


1. Cannell MB, Cheng H, Lederer WJ. The control of calcium release in heart muscle. *Science*. 1995; 268:1045–1049.
2. Cheng H, Lederer WJ, Cannell MB. Calcium Sparks - Elementary Events Underlying Excitation-Contraction Coupling in Heart-Muscle. *Science.* 1993;262:740–744.
3. Bers DM. Cardiac excitation-contraction coupling. *Nature.* 2002;415:198–205.
4. Bers DM. Calcium fluxes involved in control of cardiac myocyte contraction. *Circ Res.* 2000;87:275–281.
5. Bers DM. Calcium Signaling in Cardiac Ventricular Myocytes. *Ann NY Acad Sci.* 2005;1047:86–98.
6. Cannell MB, Kong CHT. Local control in cardiac E–C coupling. *J Mol Cell Cardiol.* 2012;52:298–303.
7. Hoang-Trong TM, Ullah A, Jafri MS. Calcium Sparks in the Heart: Dynamics and Regulation. *Res Rep Biol.* 2015;6:203–214.
8. Inoue M, Bridge JHB. Ca2+ sparks in rabbit ventricular myocytes evoked by action potentials: involvement of clusters of L-type Ca2+ channels. *Circ Res.* 2003;92:532–538.
9. Cannell MB, Cheng H, Lederer WJ. Spatial non-uniformities in [Ca2+]i during excitation-contraction coupling in cardiac myocytes. *Biophys J.* 1994;67:1942–1956.
10. Zima AV, Picht E, Bers DM, Blatter LA. Termination of cardiac Ca2+ sparks: role of intra-SR [Ca2+], release flux, and intra-SR Ca2+ diffusion. *Circ Res.* 2008;103:e105–15.
11. Crespo LM, Grantham CJ, Cannell MB. Kinetics, stoichiometry and role of the Na-Ca exchange mechanism in isolated cardiac myocytes. *Nature.* 1990;345:618–621.
12. Dibb KM, Graham HK, Venetucci LA, Eisner DA, Trafford AW. Analysis of cellular calcium fluxes in cardiac muscle to understand calcium homeostasis in the heart. *Cell Calcium.* 2007;42:503–512.
13. Bers DM, Despa S. Cardiac Myocytes Ca2+ and Na+ Regulation in Normal and Failing Hearts. *J Pharmacol Sci.* 2006;100:315–322.
14. Berlin JR, Bassani JW, Bers DM. Intrinsic cytosolic calcium buffering properties of single rat cardiac myocytes. *Biophys J.* 1994;67:1775–1787.
15. Guo T, Zhang T, Ginsburg KS, Mishra S, Brown JH, Bers DM. CaMKIIδC slows [Ca]i decline in cardiac myocytes by promoting Ca sparks. *Biophys J.* 2012;102:2461–2470.
16. Cooper PJ, Soeller C, Cannell MB. Excitation-contraction coupling in human heart failure examined by action potential clamp in rat cardiac myocytes. *J Mol Cell Cardiol.* 2010;49:911–917.
17. Song L-S, Qua Z, Karmac A. Orphaned ryanodine receptors in the failing heart. *Proc Natl Acad Sci.* 2006;103:4305.
18. Sobie EA, Song L-S, Lederer WJ. Local recovery of Ca2+ release in rat ventricular myocytes. *J Physiol.* 2005;565:441–447.
19. Brochet D, Brochet DXP, Yang D, Di Maio A, Lederer WJ, Franzini-Armstrong C, Cheng H. Ca2+ blinks: Rapid nanoscopic store calcium signaling. *Proc Natl Acad Sci.* 2005;102:3099–3104.
20. Bassani JW, Bassani RA, Bers DM. Relaxation in rabbit and rat cardiac cells: species-dependent differences in cellular mechanisms. *J Physiol.* 1994;476:279–293.
21. Grantham CJ, Cannell MB. Ca2+ influx during the cardiac action potential in guinea pig ventricular myocytes. *Circ Res.* 1996;79:194–200.
22. Yuan W, Ginsburg KS, Bers DM. Comparison of sarcolemmal calcium channel current in rabbit and rat ventricular myocytes. *J Physiol.* 1996;493:733–746.
23. Lansman JB, Hess P, Tsien RW. Blockade of current through single calcium channels by Cd2+, Mg2+, and Ca2+. *J Gen Physiol.* 1986;88:321–347.
24. Cannell MB, Berlin JR, Lederer WJ. Effect of membrane potential changes on the calcium transient in single rat cardiac muscle cells. *Science.* 1987;238:1419–1423.
25. Izu LT, Banyasz T, Balke CW, Chen-Izu Y. Eavesdropping on the social lives of Ca(2+) sparks.

*Biophys J.* 2007;93:3408–3420.
26. Cheng H, Lederer MR, Lederer WJ, Cannell MB. Calcium sparks and [Ca2+]i waves in cardiac myocytes. *Am J Physiol.* 1996;270:C148–59.
27. Wier WG, Cannell MB, Berlin JR, Marbán E, Lederer WJ. Cellular and subcellular heterogeneity of [Ca2+]i in single heart cells revealed by fura-2. *Science.* 1987;235:325–328.
28. Litwin SE, Zhang D, Bridge JH. Dyssynchronous Ca(2+) sparks in myocytes from infarcted hearts. *Circ Res.* 2000;87:1040–1047.
29. Heinzel FR, MacQuaide N, Biesmans L, Sipido K. Dyssynchrony of Ca2+ release from the sarcoplasmic reticulum as subcellular mechanism of cardiac contractile dysfunction. *J Mol Cell Cardiol.* 2011;50:390–400.
30. Ibrahim M, Gorelik J, Yacoub MH, Terracciano CM. The structure and function of cardiac t-tubules in health and disease. *Proc Biol Sci.* 2011;278:2714–2723.
31. Armoundas AA, Rose J, Aggarwal R, Stuyvers BD, O'Rourke B, Kass DA, Marban E, Shorofsky SR, Tomaselli GF, Balke CW. Cellular and molecular determinants of altered Ca2+ handling in the failing rabbit heart: primary defects in SR Ca2+ uptake and release mechanisms. *Am J Physiol Heart Circ Physiol*. 2007;292:H1607–18.
32. Belevych AE, et al. (2017) The role of spatial organization of Ca(2+) release sites in the generation of arrhythmogenic diastolic Ca(2+) release in myocytes from failing hearts. *Basic Res Cardiol* 2017;112:44.
33. Bovo E, Mazurek SR, Blatter LA, Zima AV. Regulation of sarcoplasmic reticulum $Ca^{2+}$ leak by cytosolic $Ca^{2+}$ in rabbit ventricular myocytes. *J Physiol.* 2011;589:6039–6050.

## FIGURE LEGENDS

**Figure 1. Late $Ca^{2+}$ sparks (LCS) during the decay of evoked $Ca^{2+}$ transients.**(**A**) High resolution recordings (confocal pinhole set to 1 Airy unit) of $Ca^{2+}$ release during normal $Ca^{2+}$ transients (left) at 0.5 Hz. Image enhancement by subtraction of the low-pass filtered transient shows LCS more clearly (white boxes) (right). (**B**) Comparison $Ca^{2+}$ sparks at rest (top left) and LCS (top right) showed high spatio-temporal similarity. The temporal profiles of averaged events (23 $Ca^{2+}$ sparks and 18 LCS) show LCS have a similar time course to resting $Ca^{2+}$ sparks in the same cell (bottom). (**C**) Average LCS amplitude was greater than resting $Ca^{2+}$ sparks (*p<0.05, **p<0.01, 196 LCS, 42 diastolic n/N = 12/6). (**D**) Di-8-ANEPPS labelling of t-tubules (top) was used to calculate a distance map to nearest t-tubule (middle). The line scan position is indicated by the white line and the location of LCS by white circles. LCS occurred near t-tubules and at regions with early evoked $Ca^{2+}$ release (bottom). (**E**) The median distance to nearest t-tubule was shorter for LCS sites than the cell average distance (n/N = 11/5). Kolmogorov-Smirnov test. (**F**) $Ca^{2+}$ transient latency at sites with LCS was shorter than the cell average latency (n/N = 28/8). *p<0.05.

**Figure 2. Restitution and refractory behaviour of LCS.** Time and amplitude restitution of LCS reveal their SR load dependence. (**A**) The interval of successive LCS arising from the same location (top), and their relative amplitudes were measured in background-subtracted recordings (bottom). (**B**) The probability density function of LCS following evoked $Ca^{2+}$ release was similar to the time course of the normalised average $Ca^{2+}$ transient (solid colour behind histogram bars) and decreased exponentially from the maxima (red line). (**C**) The probability of a second LCS at the same site had a similar time-dependence to the first LCS (B) (**D**) After the first LCS the amplitude of the second LCS increased with a time constant, $\tau$ = 77 ms. (**E**) The probability of LCS activation ($P_{LCS}$) was essentially the same following evoked $Ca^{2+}$ release (red) or after a prior LCS (blue) (p = 0.86, extra sum-of-squares F test). (B) 350 LCS from n/N = 19/9, (C&D) 79 LCS pairs from n/N = 10/8.

**Figure 3. Effects of LTCC block reveals additional triggers for LCS**. Blocking LTCC before or after evoked $Ca^{2+}$ release shows LCS can be triggered by late LTCC activity. (**A**) Line scan recordings of consecutive $Ca^{2+}$ transients in normal Tyrode's (NT) and in NT + 10 µmol/L $Cd^{2+}$. The extracellular solution was rapidly changed between contractions to preserve SR load. $Cd^{2+}$ application produced more spatial non-uniformities in early $Ca^{2+}$ release and increased the number of LCS. (**B**) The $Ca^{2+}$ transient decay was clearly delayed in $Cd^{2+}$. (**C**) $Cd^{2+}$ increased mean LCS frequency by ~40 %. (**D**) $Cd^{2+}$ slightly decreased the $Ca^{2+}$ transient amplitude and (**E**) increased its duration compared to NT. (**F**) Rapid application of NT + 100 µmol/L $Cd^{2+}$ (after the $Ca^{2+}$ transient upstroke) preserved early $Ca^{2+}$ release but decreased the number of LCS. (**G**) The $Ca^{2+}$ transient upstroke was preserved in $Cd^{2+}$ (green line) compared to NT (blue). (**H**) Mean LCS frequency was reduced by ~40 % by $Cd^{2+}$. (**I**) Average $Ca^{2+}$ transient amplitude was not reduced by rapid $Cd^{2+}$ application while the $Ca^{2+}$ transient duration was decreased slightly (**J**) (p = 0.05). (C-E) n/N = 15/5, (H-J) n/N = 12/4. **p<0.01, ***p<0.001 paired t-test.

**Figure 4. Late $Ca^{2+}$ sparks can interact to form "$Ca^{2+}$ ripples".** (**A**) Unprocessed high resolution recording showing multiple LCS. (**B**) The autocorrelogram of (A) reveals the time-dependence between repeating events (indicated by yellow arrow), with a mean delay of 145 ms, as highlighted in (**C**). (**D**) (left) Further pacing resulted in increased $Ca^{2+}$ load and many more LCS. The right panel emphasizes how LCS appear to trigger additional sites forming multiple propagating $Ca^{2+}$ ripples (marked by yellow chevron overlays). (**E**) The 2D autocorrelogram shows that some LCS have both temporal and spatial relationships to other LCS. (**F**) Calculation of propagation velocities in the 2D autocorrelation showed a dominant peak at ~114 µm/s. Points indicated in (C) and (F) were highly significant ($p < 10^{-5}$) (blue lines show mean ± 5SD of scrambled data).

## NOVELTY AND SIGNIFICANCE

### *What Is Known?*

- $Ca^{2+}$ transients are due to near-synchronous $Ca^{2+}$ release from internal stores soon after the upstroke of the action potential.
- $Ca^{2+}$ changes during the $Ca^{2+}$ transient reflect the balance of release and uptake mechanisms with the latter dominating the time course of the decline in $Ca^{2+}$.
- $Ca^{2+}$ dysregulation in cardiac muscle cells influences contraction strength and can promote fatal arrhythmias

### *What New Information Does This Article Contribute?*

- Late $Ca^{2+}$ release events in the form of "late $Ca^{2+}$ sparks" (LCS) can occur during the $Ca^{2+}$ transient and delay its decay.
- LCS arise from $Ca^{2+}$ release sites that have recovered from their earlier activation and are triggered by late opening(s) of $Ca^{2+}$ channels and by cytosolic $Ca^{2+}$ itself.
- LCS can produce microscopic waves of $Ca^{2+}$ release ("$Ca^{2+}$ ripples") by partially regenerative, sequential, LCS activation which may further prolong the $Ca^{2+}$ transient.

$Ca^{2+}$ regulation in cardiac muscle cells critically influences the contraction and electrical activity of the heart. The near-synchronous cell-wide activation of $Ca^{2+}$ sparks early during an action potential produces the $Ca^{2+}$ transient upstroke. Consequent depletion of $Ca^{2+}$ stores inhibits further $Ca^{2+}$ release, so $Ca^{2+}$ removal pathways are generally thought to determine the time course of $Ca^{2+}$ transient decay and restoration of resting conditions. Release sites which fail to activate, or recover more quickly from prior release, could be activated to slow the $Ca^{2+}$ transient decay and promote electrical instability. Using high resolution recordings, novel late $Ca^{2+}$ sparks (LCS) were detected during action potential-evoked $Ca^{2+}$ transients. LCS were triggered by late $Ca^{2+}$ channel openings as well as the increased cytosolic $Ca^{2+}$ during the $Ca^{2+}$ transient. Partial inhibition of surface membrane $Ca^{2+}$ current paradoxically increased LCS production. LCS will slow the $Ca^{2+}$ transient decay and may even interact to form microscopic propagating $Ca^{2+}$ release events ("$Ca^{2+}$ ripples"). $Ca^{2+}$ ripples could be a substrate for abnormal electrical activity, therefore strategies which modulate LCS production may have future clinical relevance.

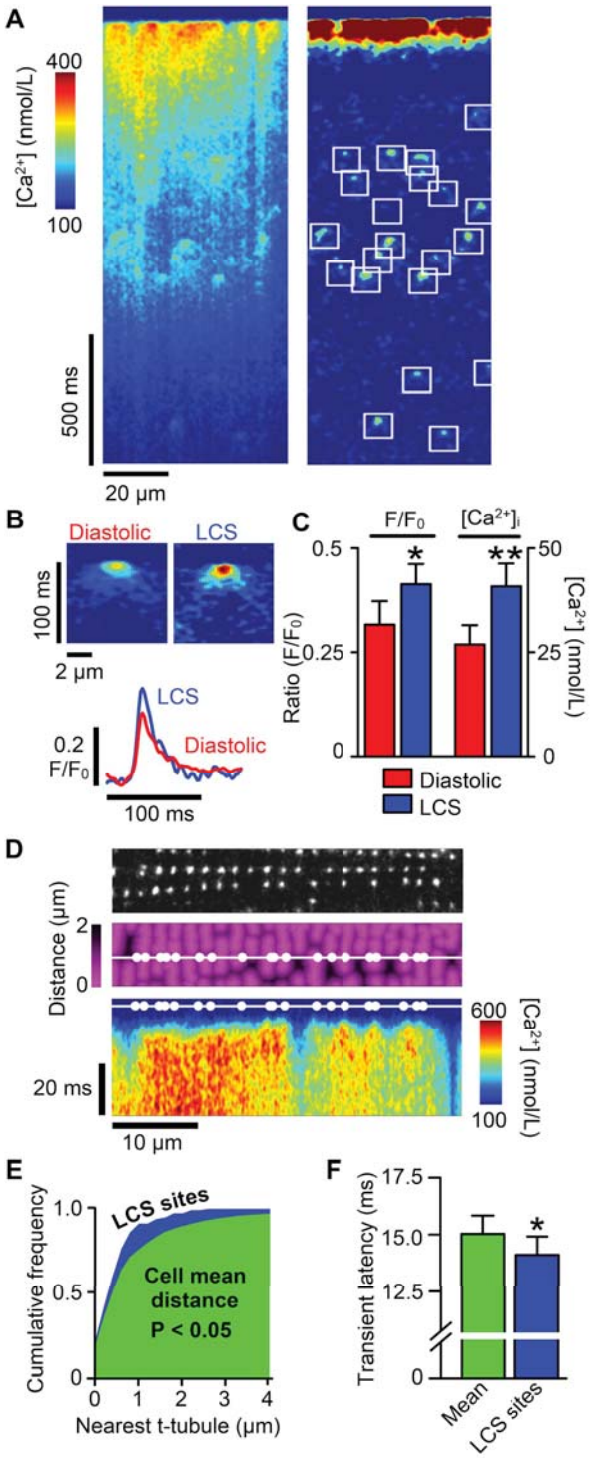

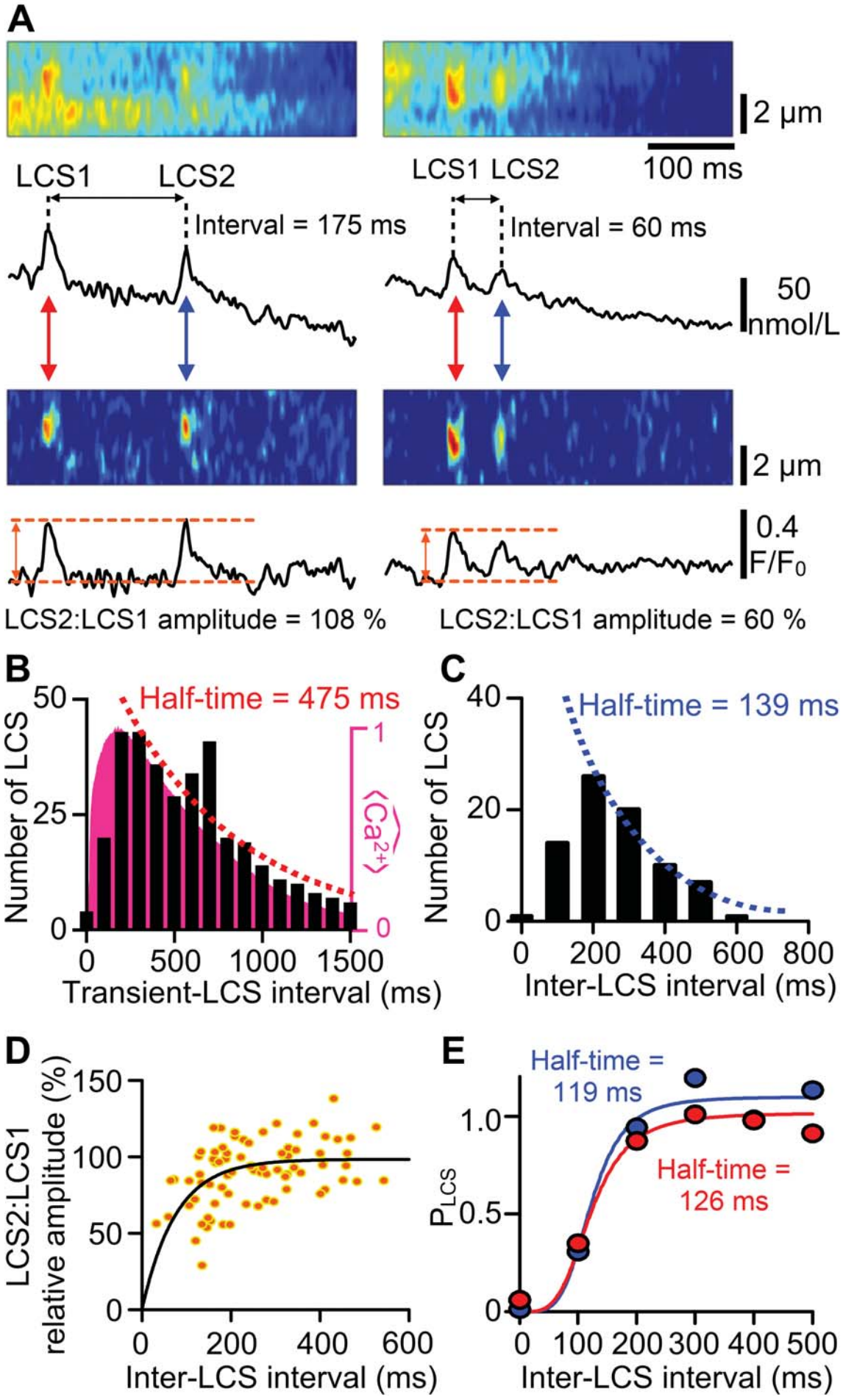

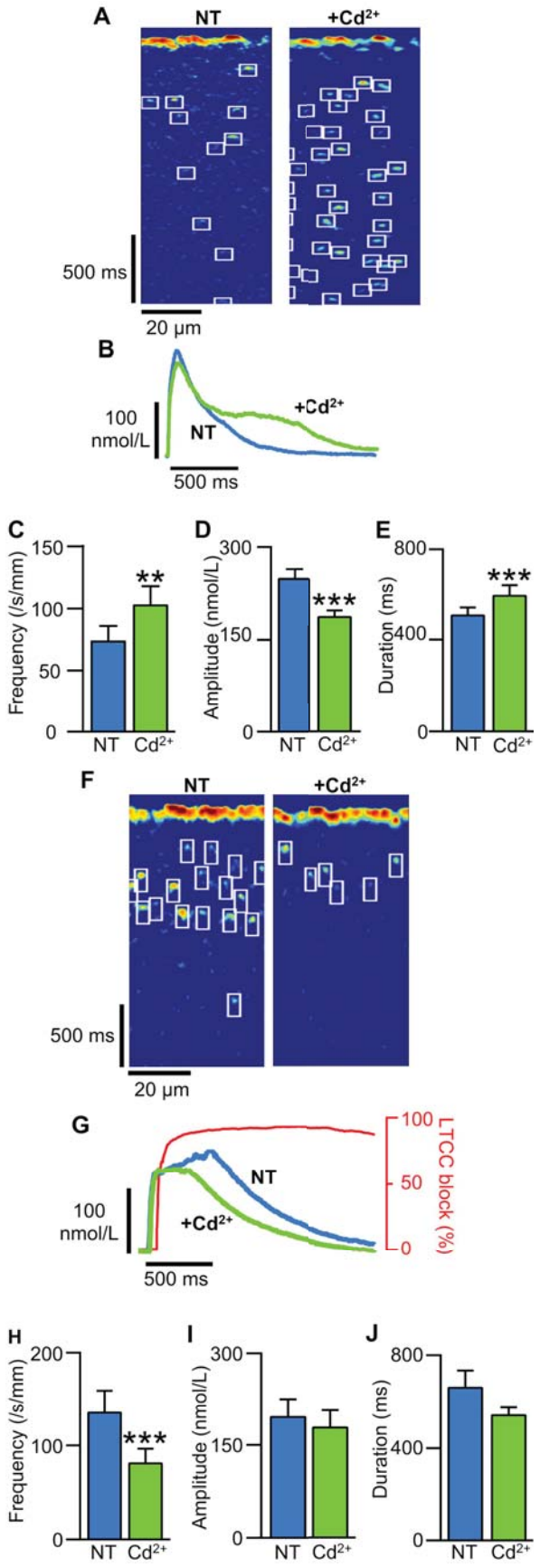

FIGURE 4

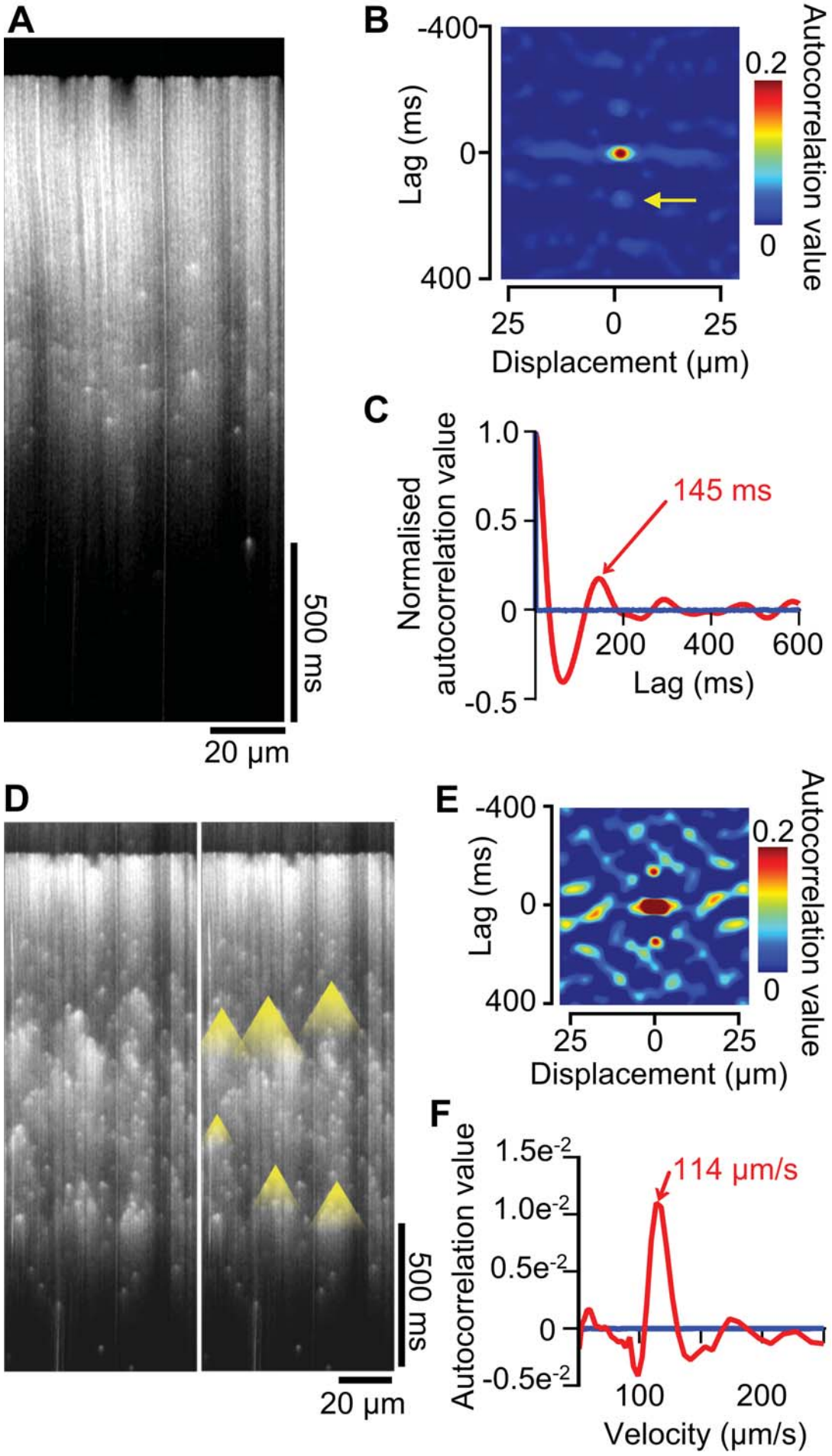

Circulation Research
JOURNAL OF THE AMERICAN HEART ASSOCIATION

# Late $Ca^{2+}$ Sparks and Ripples During the Systolic $Ca^{2+}$ Transient in Heart Muscle Cells

Ewan D Fowler, Cherrie H Kong, Jules Hancox and Mark B Cannell

*Circ Res.* published online December 27, 2017;
*Circulation Research* is published by the American Heart Association, 7272 Greenville Avenue, Dallas, TX 75231

Print ISSN: 0009-7330. Online ISSN: 1524-4571

**SUPPLEMENTAL MATERIAL**

## Detailed Methods

Animals

All experiments were performed in accordance with the UK Home Office Animals (Scientific Procedures) Act 1986 and with approval by the University of Bristol ethics committee. Left ventricular epicardial myocytes were obtained from adult male New Zealand white rabbit (2-2.5 kg) hearts after full anaesthesia (50 mg/kg sodium pentobarbital i.v.) and euthanasia. Enzymatic dissociation was carried out using 1 mg/ml collagenase II (Worthington), 0.05 mg/ml protease (type XIV Sigma) and 0.1 mmol/L $Ca^{2+}$, as described previously (1).

Solution changes and local perfusion

Experiments were performed in a modified Tyrode's solution (NT) (containing, in mmol/L: 133 NaCl, 5 KCl, 1 $NaH_2PO_4$, 10 HEPES, 10 glucose, 1.8 $CaCl_2$, 1 $MgCl_2$, pH 7.4 with NaOH) at 22±1°C. Solution changes were performed by local superfusion of cells in the recording chamber. A pressurized micropipette and a custom-made valve system allowed rapid exchange (half time < 40 ms) of the cell bathing solution synchronised to electrical stimulation. The superfusion pipette contained NT solution supplemented with 10 or 100 µmol/L $CdCl_2$ (from a 10 mmol/L stock in water) and 1 µmol/L sulforhodamine B. The time course of solution exchange was monitored during $Ca^{2+}$ line scan recordings by alternating the excitation wavelength between 488 and 543 nm for each line, while collecting emission at 492-600 and >600 nm.

The fractional block of LTCC by $Cd^{2+}$ was calculated from the Hill equation with half-maximal inhibition occurring at 2.14 µmol/L and a Hill coefficient of 0.74 (2). The onset of LTCC block during solution exchange was calculated from the normalised change in the sulforhodamine B fluorescence signal. Note that $Cd^{2+}$ is a weak blocker of NCX (by <1 % and 15 %, at 10 and 100 µmol/L respectively (2)) and TTX-sensitive $Na^+$ channels (by <1 % and 23 %, at 10 and 100 µmol/L respectively (3)). $Cd^{2+}$ was chosen over organic pharmacological blockers because LTCC block by $Cd^{2+}$ is rapid and not voltage or use-dependent.

Confocal $Ca^{2+}$ line scan recording

Cells were loaded with 5 µmol/L Fluo-4-AM for 15 min, washed in NT and then allowed to rested for >10 min to allow time for de-esterification. $Ca^{2+}$ sparks and transients were recorded in line scan mode using an inverted confocal microscope (LSM 880, Zeiss) with a 1.4 NA 63x oil immersion lens. Excitation light was provided by a 488 nm argon laser and fluorescence emission collected at 492-600 nm. $Ca^{2+}$ line scans were recorded with the pinhole set to <2 Airy units, at a pixel size of 0.1-0.2 µm/pixel and with a scan speed of 1-2 ms per line. GaAsP photodetectors were used to increase the sensitivity of $Ca^{2+}$ spark detection. $Ca^{2+}$ line scans were recorded with the pinhole set to <2 Airy units, pixel size <0.2 µm/pixel and scan speed of 1-2 ms/line. The local concentration of $Cd^{2+}$ was measured from the included sulforhodamine-B fluorescence which was excited at 543 nm and emission at >600 nm.

Fluorescence image processing

Non-cell background fluorescence from an area adjacent to the cell was subtracted from recordings. Variations in fluorescence due to dye loading was minimised by normalising fluorescence (F) to resting fluorescence during a 100 ms quiescent period immediately before stimulation ($F_0$). The $F/F_0$ recording was converted into units of $[Ca^{2+}]$ using the self-ratio method (4):

$$[Ca^{2+}]_i = \frac{KR}{(K/[Ca^{2+}]_{rest}) - R + 1}$$

Where *K* is the *in vivo* affinity of Fluo-4 for $Ca^{2+}$ ($K_d$ ~1000 nmol/L), *R* is the self-ratio fluorescence ($F/F_0$), and $[Ca^{2+}]_{rest}$ is the resting $Ca^{2+}$ concentration (~100 nmol/L) (5).

During systolic $Ca^{2+}$ transients, the increased cytosolic $[Ca^{2+}]$ presents a challenge for the detection of LCS due to the reduced contrast of fluorescent $Ca^{2+}$ dyes at high cytosolic $[Ca^{2+}]$. To partially ameliorate this problem, the low-frequency time-averaged fluorescence in x*t* line scan recordings was subtracted from the $F/F_0$ recording. A low-pass quadratic Savitsky-Golay filter (window size ~301 ms) was applied along the *t* dimension, for every point in the *x* dimension. These filter values were found to effectively suppress background fluorescence variation due to the underlying $Ca^{2+}$ transient, while preserving the morphology and enhancing detectability of LCS.

$Ca^{2+}$ spark detection

$Ca^{2+}$ sparks were detected using an automated optimal filter algorithm implemented in MATLAB (described in detail elsewhere (6)). Briefly, the algorithm cross-correlated the flattened line scan recording with a model $Ca^{2+}$ spark and the location with the greatest correlation was identified. Following a test for significance, the centroid and amplitude of the underlying $Ca^{2+}$ spark was then measured and recorded. The $Ca^{2+}$ spark identification process was repeated until the significance of the maximum correlation fell below the threshold of significance. $Ca^{2+}$ spark full-width at half maximum and full-duration at half maximum were measured in the flattened line scan recordings. $Ca^{2+}$ spark amplitude was measured in the original $F/F_0$ or $[Ca^{2+}]$ line scan recordings at the location of detected $Ca^{2+}$ sparks.

$Ca^{2+}$ transient analysis

$Ca^{2+}$ transient latency was defined as the time between electrical stimulation and when cytosolic $[Ca^{2+}]$ was >5 standard deviations above the resting $Ca^{2+}$ signal. $Ca^{2+}$ transient latency was measured at every point along the scan line. $Ca^{2+}$ transient duration was measured as the full-duration at half maximal fluorescence (time from 50 % peak to 50 % decay of the $Ca^{2+}$ transient).

T-tubule imaging and processing

The t-tubule system in the area surrounding the $Ca^{2+}$ line scan recording was imaged by labelling the sarcolemma with di-8-ANEPPS from a stock 1 mmol/L solution (in DMSO) added directly to the cell recording chamber (final concentration 1 μmol/L) for 2-3 min. A stack of *xy* images above and below the recording focal plane was recorded using 488 nm excitation and emission collected at >600 nm.

3D stacks of t-tubule images were deconvolved using a model point spread function for the microscope objective which was derived from images of 100 nm fluorescent beads. A 3D t-tubule detection algorithm was implemented in MATLAB by the authors (who can be contacted for further details). The resulting data was then skeletonized in 3D in MATLAB (Skeleton 3D, version 1.12).

The origin of $Ca^{2+}$ sparks in three dimensions (*xyz*) is uncertain in line scanning due to the spatial spread of $Ca^{2+}$ sparks from sites just outside the scanned line. To minimize this problem, the t-tubule skeleton was collapsed to form a maximal intensity projection of the region ±2 μm above and below, and ±1 μm adjacent to the line scan region to capture the possible location of all closely coupled jSR release sites. The Euclidean distance from the apparent LCS centroid to nearest t-tubule was calculated from this maximal intensity projection.

LCS propagation/interaction analysis using 2D autocorrelation

2D autocorrelation was used to analyze the temporal and spatial relations between late $Ca^{2+}$ sparks and $Ca^{2+}$ ripples in $Ca^{2+}$ line scan records. The autocorrelogram axes represent time (lag) and space (displacement), hence the distance and angle of structures relative to the origin of the autocorrelogram corresponds to the dominant frequency and velocity of LCS propagation in the form of $Ca^{2+}$ ripples. The autocorrelation values in the time domain were measured from the origin and normalised to the autocorrelation value at the origin. The angle from the origin to the peaks of the autocorrelation correspond to propagation velocities of $Ca^{2+}$ ripples (~50-250 μm/s).

To test whether the apparent peaks in the autocorrelogram were significant, we scrambled the data and repeated the autocorrelation. This was repeated 5 times to compute a mean and standard deviation for equivalent uncorrelated data.

Statistical Analysis

Data were tested for normality using the Shapiro-Wilk test and in cases where data were skewed, the test was reapplied to log-transformed data. Paired t-tests were performed on normally distributed original data or the transformed data. Differences between cumulative frequencies were tested using the Kolmogorov-Smirnov test. Curve fits of LCS probability ($P_{LCS}$) were compared using the extra sum-of-squares F test. Results are presented as mean ± SEM. The number of cells (n) and animals (N) used for each experiment are given in figure legends as n/N. $p<0.05$ was considered to be the limit of statistical confidence. A nested hierarchical approach was used to examine possible clustering effects in Fig. 1 and the ICC was found to be only 0.14 (7).

**Supplemental Text**

Effects of BDM.

BDM is not a specific inhibitor of muscle contraction (8) and partially inhibits many of the key $Ca^{2+}$ transport systems in cardiomyocytes. It has been shown to affect NCX (9), $Ca^{2+}$ channels (10) and weakly enhances PP1 and/or PP2A phosphatase activity (the latter at 100 mmol/l) (11). A reduction in LTCC availability should increase the probability of LCS as shown in Fig. 3a. On the other hand, 10 mM BDM can reduce SR $Ca^{2+}$ content with only small effects on the amplitude of the $Ca^{2+}$ transient (12). Therefore, BDM may alter the exact relationship between triggers and the consequent $Ca^{2+}$ release but is clearly not the cause of LCS activity seen here (see Online Figure I).

**Supplemental Figures and Figure Legends**

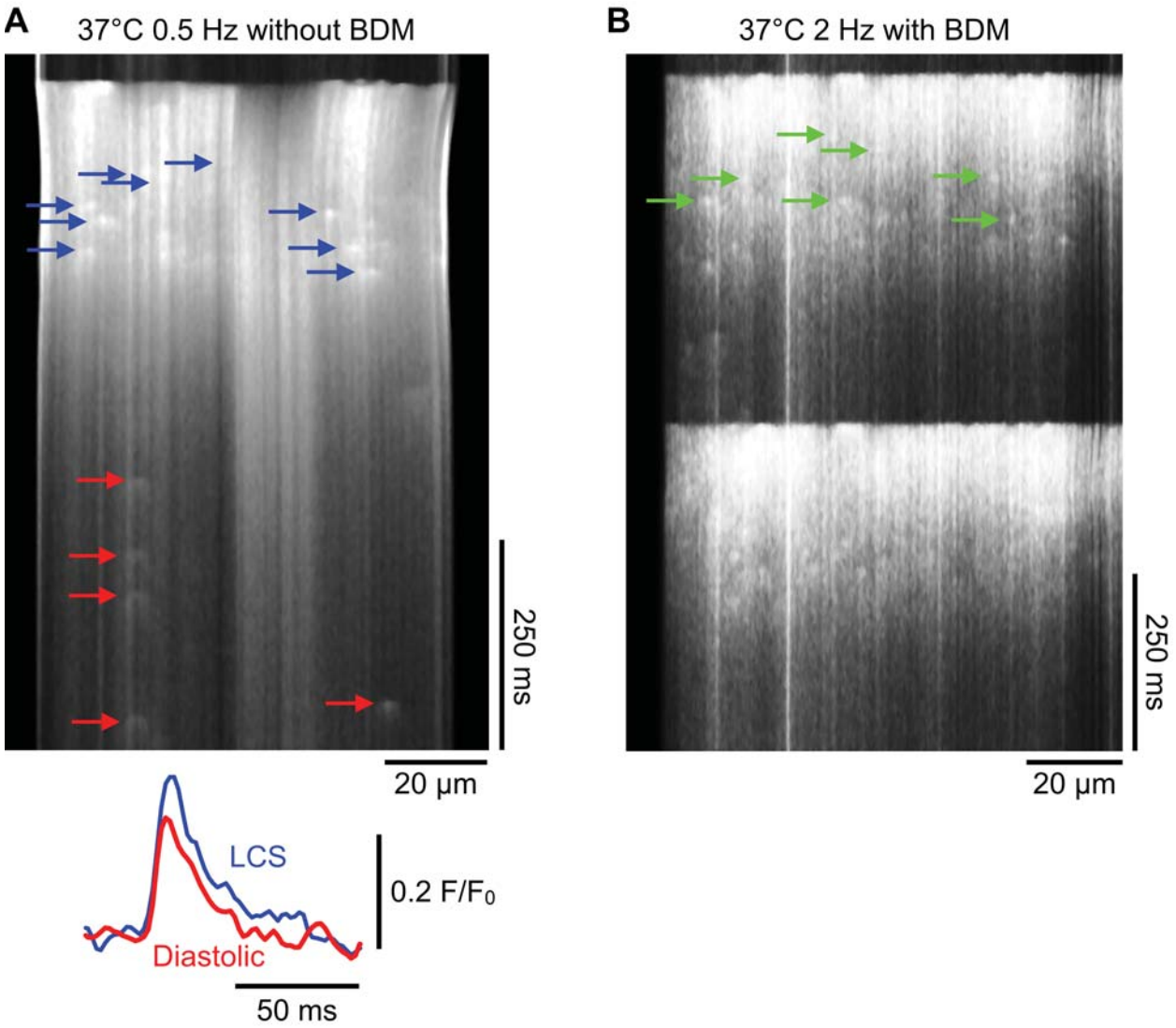


**Online Figure I . Examples of LCS production at 37°C.** The left hand panel shows unprocessed data in the absence of BDM with some clear LCS indicated by blue arrows. Note the presence of a movement artifact showing the contraction of the cell. For comparison, some diastolic $Ca^{2+}$ sparks are also indicated (red arrows). Plots of average amplitudes show similar behavior to the data shown in Figure 1. On the right, the pacing rate was increased to 2Hz at 37°C (with BDM to avoid the movement artifact) and, while the increased $Ca^{2+}$ transient amplitude decreases contrast and increases Poisson noise, LCS can still be discerned.

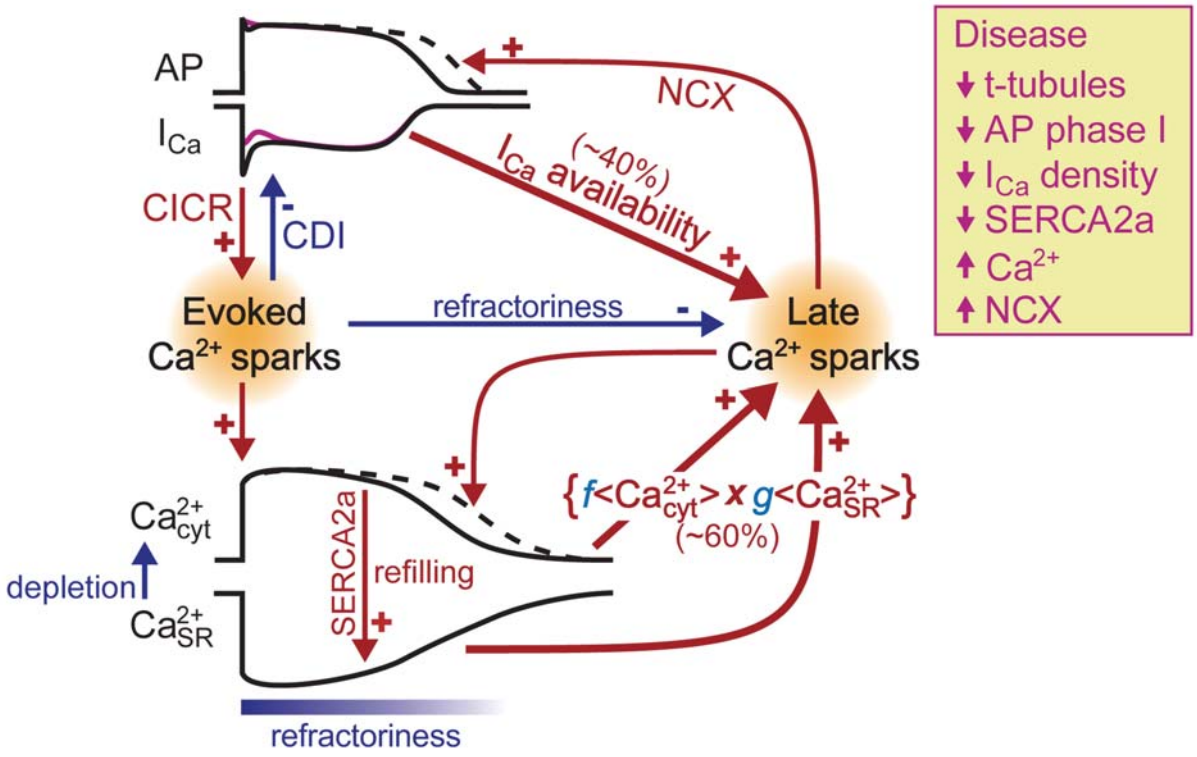


**Online Figure II. Mechanisms for interactions between $Ca^{2+}$ sparks, LCS and the ECC cycle**. During the cardiac AP, $Ca^{2+}$ enters the cell via LTCC (seen macroscopically as $I_{Ca}$) which causes the near-synchronous release of $Ca^{2+}$ from jSR by $Ca^{2+}$ -induced $Ca^{2+}$ release (CICR). Activated SR junctions enter a refractory state where further release is prevented due to depletion of SR $Ca^{2+}$. $Ca^{2+}$ -dependent inactivation (CDI) of LTCC may also decrease the probability of LCS. Cytosolic $Ca^{2+}$ is re- sequestered by SERCA2a, refilling the SR. During the AP plateau, LTCC may (re-)open and may trigger LCS if the SR release sites were triggered during the AP or else recovered from the refractory state. Inward current generated by NCX will prolong the AP and increase the duration of $I_{Ca}$. By delaying the decline of the $Ca^{2+}$ transient, LCS may promote additional LCS which may take the form of $Ca^{2+}$ ripples, if SR load is sufficient and SR release not refractory. The non- LTCC triggered probability of LCS triggering can be described by an equation of the form f<$Ca^{2+}_{cyt}$> x g< $Ca^{2+}_{SR}$> where f and g describe the cytosolic and SR dependencies of $Ca^{2+}$ spark initiation. This may account for ~60% of LCS in normal cells (the remainder being due to LTCC activity). In disease, the pathological changes in the ECC cycle can increase the probability of LCS which, in turn, may prolong the duration of the $Ca^{2+}$ transient and AP duration forming a new positive feedback pathway.

## Supplemental References

1. Cooper PJ, Soeller C, Cannell MB. Excitation-contraction coupling in human heart failure examined by action potential clamp in rat cardiac myocytes. *J Mol Cell Cardiol* 2010;49:911–917.

2. Hobai IA, Bates JA, Howarth FC, Levi AJ. Inhibition by external Cd2+ of Na/Ca exchange and L-type Ca channel in rabbit ventricular myocytes. *Am J Physiol: Heart Circ Physiol* 1997;272:H2164–H2172.

3. DiFrancesco D, Ferroni A, Visentin S, Zaza A. Cadmium-induced blockade of the cardiac fast Na channels in calf Purkinje fibres. *Proc Roy Soc Lond, B* 1985;223:475–484.

4. Cannell MB, Cheng H, Lederer WJ. Spatial non-uniformities in [Ca2+]i during excitation-contraction coupling in cardiac myocytes. *Biophys J* 1994;67:1942–1956.

5. Wier WG, Cannell MB, Berlin JR, Marbán E, Lederer WJ. Cellular and subcellular heterogeneity of [Ca2+]i in single heart cells revealed by fura-2. *Science* 1987;235:325–328.

6. Kong CHT, Soeller C, Cannell MB. Increasing Sensitivity of Ca2+ Spark Detection in Noisy Images by Application of a Matched-Filter Object Detection Algorithm. *Biophys J* 2008;95(12):6016–6024.

7. Sikkel MB, Francis DP, Howard J, Gordon F, Rowlands C, Peters NS, Lyon AR, Harding SE, MacLeod KT. Hierarchical statistical techniques are necessary to draw reliable conclusions from analysis of isolated cardiomyocyte studies. *Cardiovasc Res*. 2017;113:1743–1752. doi:10.1093/cvr/cvx151.

8. Sellin LC, McArdle JJ. Multiple effects of 2,3-butanedione monoxime. *Pharmacol Toxicol* 1994;74(6):305–313.

9. Watanabe Y, Iwamoto T, Matsuoka I, Ohkubo S, Ono T, Watano T, Shigekawa M, Kimura J. Inhibitory effect of 2,3-butanedione monoxime (BDM) on Na(+)/Ca(2+) exchange current in guinea-pig cardiac ventricular myocytes. *Br J Pharmacol*. 2001;132:1317–1325.

10. Chapman RA. The effect of oximes on the dihydropyridine-sensitive Ca current of isolated guinea-pig ventricular myocytes. *Pflugers Arch* 1993;422:325–331.

11. Zimmermann N, Boknik P, Gams E, Gsell S, Jones LR, Maas R, Neumann J, Scholz H. Mechanisms of the contractile effects of 2,3-butanedione-monoxime in the mammalian heart. *Naunyn-Schmied Arch Pharmacol*. 1996;354:431–436.

12. Adams W, Trafford AW, Eisner DA. 2,3-Butanedione monoxime (BDM) decreases sarcoplasmic reticulum Ca content by stimulating Ca release in isolated rat ventricular myocytes. *Pflugers Arch* 1998;436:776–781.